Performance-based reliability assessment of quay walls

Hao, Na; Duffy, Kevin; Reale, Cormac; Gavin, Kenneth

DOI
10.1016/j.compgeo.2025.107794

Publication date
2025

Document Version
Final published version

Published in
Computers and Geotechnics

Computers and Geotechnics 191 (2026) 107794

Contents lists available at ScienceDirect

Computers and Geotechnics

journal homepage: www.elsevier.com/locate/compgeo

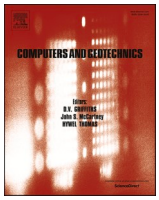

Performance-based reliability assessment of quay walls

Na Hao [a,*], Kevin Duffy [a], Cormac Reale [b], Kenneth Gavin [a]

[a] Department of Geoscience & Engineering, TU Delft, the Netherlands
[b] Department of Architecture and Civil Engineering, University of Bath, United Kingdom

ARTICLE INFO

Keywords:
Quay wall
Reliability analysis
Cone penetration testing
Field monitoring
Numerical modelling

ABSTRACT

Functional demands on quay walls are steadily rising with increases in both ship size and the frequency of port calls, requiring robust safety and performance assessment frameworks. Most existing studies on quay walls remain constrained by simplified analytical or numerical models, limited consideration of failure modes, insufficient model validation, and the absence of site-specific soil correlation, making it difficult to assess real structures under realistic loading conditions. This study presents a novel Cone Penetration Tests (CPT)-driven, performance-based reliability framework that samples directly from measured CPT distributions to preserve field consistent parameter relationships without requiring site-specific covariance matrices. The framework is demonstrated on a recently constructed, full-scale instrumented quay wall in the Port of Rotterdam. A two-dimensional finite element model with the Hardening Soil Small-strain (HSS) formulation is calibrated against construction-stage monitoring (wall deformations and anchor forces) and coupled to a probabilistic engine to evaluate multiple ultimate and serviceability limit states through an explicit failure tree.

Results indicate that the structural failure of the wall governs the overall reliability of the quay wall, while wall deformation is the most variable response requiring close monitoring. Sensitivity analyses reveal that deeper dredging and higher surcharge loads markedly reduce reliability with wall structural failure governing and serviceability limit states showing the highest sensitivity to these hypothetical changes. The proposed approach provides a generalisable CPT-based methodology for reliability assessment of geotechnical structures based on site investigation data and monitoring data, supporting more informed, data-driven decision-making in design, and life-cycle management.

1. Introduction

The operational demands on port infrastructure are continuously evolving over their service life. Driven by increases in trade and globalisation, ship size has quadrupled since the 1990 s (Ge et al., 2021), placing ever-greater demands on quay walls. Quay walls provide berthing space for ships and facilitate the loading and unloading of cargo. The variability in operational demands, soil conditions, and nautical conditions means that quay walls within even just a single port can vary greatly in size and shape in order to maximise design efficiency at a given site (de Gijt and Broeken, 2013). Typically, quay walls comprise different retaining structures, anchorage systems, and foundation types, all interacting through complex soil-structure mechanisms.

Finite element (FE) methods are widely used to capture the nonlinear soil behaviour and complex soil-structure interaction mechanisms governing quay wall performance (Alesiani and Ruggeri, 2024; Roubos et al., 2021; Tan et al., 2018). However, finite element methods are deterministic in nature, failing to reflect the complex variations in soil and loading conditions across a quay wall, often spanning hundreds of metres in length. To address this, finite element methods are sometimes coupled with reliability toolboxes or probabilistic interfaces, such as for deep excavations (Ene et al., 2021; Momeni et al., 2021; Rippi and Teixeira, 2016), slopes and embankments (de Gast et al., 2021; Reale et al., 2015; Rippi et al., 2016; Hao et al., 2022). For quay walls, a limited number of studies have demonstrated promising results (Post et al., 2021; Roubos et al., 2021; Hemel et al., 2024; Wolters et al., 2013), but most rely on simplified models or focus on individual failure modes without establishing a comprehensive failure tree. A framework of finite-element based reliability assessment of quay wall which can reveal failure probabilities and dominant failure modes, enabling targeted maintenance and renovation strategies is necessary (Armstrong et al., 2024; Bauduin et al., 2017; Otake and Honjo, 2022; Phoon, 2023).

Inevitably, the accuracy of these assessments depends on the quality of the underlying numerical model. However, obtaining a reliable

* Corresponding author.
E-mail address: n.hao@tudelft.nl (N. Hao).

https://doi.org/10.1016/j.compgeo.2025.107794
Received 13 August 2025; Received in revised form 3 November 2025; Accepted 20 November 2025
Available online 24 November 2025

benchmark numerical model that is validated by real-world data remains a significant challenge for quay walls. Full-scale load tests are the most optimal form of validation but are rarely feasible due to their cost and complexity (Alesiani and Ruggeri, 2024; Feremans and Vanhooydonck, 2019; Hemel, 2023; Segato et al., 2010). Nevertheless, the increasing development of 'smart quay walls' (Voogt, 2023) provides new opportunities, since the large deformations during construction can be used to validate the model.

A previous study (Roubos et al., 2021) into quay walls in Rotterdam has shown that time-independent variables, such as the soil and structural properties, tend to dominate reliability indices. With this in mind, this study takes a recently constructed quay wall in the port of Rotterdam, and uses an extensive Cone Penetration Tests (CPT) investigation programme to improve the understanding of the in-situ conditions and spatial variability across long, linear infrastructure like quay walls. The proposed framework directly samples from measured CPT distributions, preserving field-consistent parameter relationships and capturing in-situ spatial variability in a statistically rigorous way. The model was validated by an extensive set of measurements performed on the quay wall during construction and staged dredging. The validated model is then used to assess current performance, quantify the impact of spatial averaging, and evaluate the structural implications of hypothetical operational changes. The study concludes with recommendations on quay wall performance, the influence of spatial averaging and and potential remediation measures.

2. Quay wall example

The quay wall is a 1.4 km long terminal in the port of Rotterdam and is divided into several different sections to accommodate for different types of ships and berthing operations. A single, well-instrumented cross-section of the quay wall was taken, forming part of a tank terminal that can facilitate the berthing and unloading of VLCC (Very Large Crude Carrier) class ships. Additional details on the monitoring data and finite element model has also been presented in Lai et al., (2025) who examined the applicability of a CPT-based deterministic finite element model.

2.1. Ground conditions

Nearly two hundred cone penetration tests were conducted along the entire length of the quay wall, as well as fifteen boreholes. For the analysis, fifteen CPTs around the section-of-interest—both waterside and landside—were taken. The CPT profiles are shown in Fig. 1 in grey, as well as the average cone resistance in green. The CPT has been discretised into Ground Units (GU) based on their engineering relevance for the study:

- **+5m to 0 m, GU1:** Backfill SAND, reworked and redeposited during construction.
- **0 m to − 13 m, GU2:** Anthropogenic dense fine to coarse medium SAND, with average CPT cone tip resistances q_c of 19 MPa
- **−13.0 m to − 19.0 m, GU3:** Medium dense to dense silty fine SAND (Naaldwijk and Echteld Formations), deposited during the Holocene epoch. Locally with clayey and silty pockets.
- **−19.0 m to − 22.0 m, GU4:** Stiff CLAY (Wijchen Member, Kreftenheye Formation), deposited during the late-Pleistocene.
- **−22.0 m to − 45.0 m, GU5:** Dense to very dense slightly gravelly coarse SAND (Kreftenheye Formation), fluvially deposited during the late-Pleistocene.

2.2. Quay wall

With a total height of 42 m, the quay wall consists of four primary components (Fig. 1): the combined wall, the superstructure, a row of Müller Verpress (MV) anchors and two rows of the screw injection (SI) piles. The combined wall derives most of its stiffness from 1.4 m diameter driven open-ended piles, spaced at 3.3 m centre-to-centre (Fig. 2). Sheet piles span between the open-ended piles, preventing soil flow through the wall and into the sea. Sitting on top of the combined wall is the concrete superstructure, cast in 23 m long segments. The relieving platform forms part of this superstructure—a two-metre-thick slab that uses the weight of the overlying soil to resist overturning moments, sometimes referred to as a "Danish quay wall" (Bokhoven, 1966; Ruggeri et al., 2019).

The MV anchors are tied in directly at the front concrete wall. These anchors are large steel I-beams (0.6 × 0.3 m in size; 3.3 m centre-to-centre) that were installed through a combination of hammering and grout injection from the anchor tip. Screw injection piles (850 mm in diameter), support the underside of the relieving platform and were installed using a combination of screw-in torque and grout injection (Duffy et al., 2024a). The design capacities for the anchors and

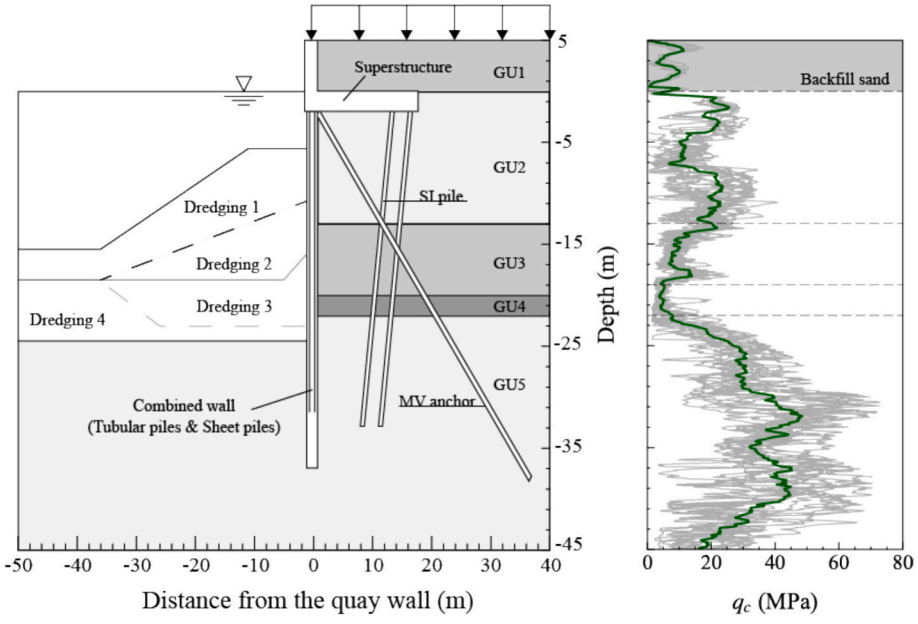

Fig. 1. Quay wall and CPT profiles made prior to construction.

Fig. 2. Construction of the quay wall (a) installation of the MV anchors; (b) installation of the tubular piles in the combined wall; (c) casting of the superstructure segments; (d) dredging.

compression piles are 7 MN and 5.5 MN respectively.

The quay wall is designed for a seabed depth of at least − 25.6 m, with a guaranteed nautical depth of − 23.6 m (which accounts for dredging tolerances, scour protection and sedimentation over the quay wall's lifetime). A design surcharge load of 40 kPa was assumed, of which 30 % is permanent loading and 70 % is variable loading. This load is applied over the entire upper surface from the seaside to storage tanks set back 47 m from the front of the wall.

2.3. Construction monitoring

Construction of the quay wall was performed on dry land, lasting fourteen months in total. Following the completion of main structure, dredging in front of the wall proceeded incrementally in four main stages, labelled Dredging 1 to Dredging 4 (Fig. 1), leading to a final seabed depth of − 24.5 m at the cross-section-of-interest. These dredged depths were recorded weekly with multibeam echo sounders, and were generally to a tolerance of ± 0.5 m.

The quay wall was instrumented at several locations to monitor deformations and loads during construction, and later during the operational life of the structure. At the cross-section of interest this included:

- **Fiber Bragg Grating (FBG) strain sensors** at the top of the MV anchor, two on each flange and one in the centre of the web to assess bending effects, along with one temperature sensor to compensate for temperature fluctuations. Strain was then converted to a normal force using the cross-sectional stiffness of the anchor. Measurement frequency was once every hour.
- **Manual inclinometers** measured the lateral deformation of the entire wall through a casing cast directly into the superstructure and along the length of an open-ended pile in the combined wall. These measurements were made at pre-defined intervals after each dredging phase.

3. Finite element-based reliability analysis

Typically finite element reliability assessments consider either i) strength and stiffness random variables independently from one another, or ii) calculate the site-specific covariance of the underlying random variables. Both methods have their drawbacks as the former negates the reality of soil behaviour and can allow unrealistic realisations to develop where random variables have inadmissible values relative to each other, while the latter requires extensive site-specific datasets to ensure accuracy.

This study sets out an approach where CPT measurements are directly considered as stochastic input variables instead of constitutive parameters (Fig. 3). For each realisation, values of cone resistance (q_c) and sleeve friction (f_s) are generated based on measured distributions. These profiles are then transformed into the required constitutive model inputs using CPT correlations, see Table 2. The advantage of this approach is that each realisation is consistent with real field data, avoiding unrealistic soil parameter combinations. Additionally, the

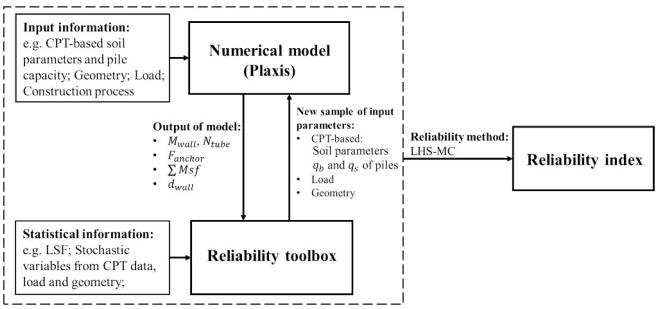

Fig. 3. Reliability interface of CPT-based finite element reliability assessment.

Table 1
Statistical summary of the input variables.

Variables	Unit	Average	Standard deviation	CoV	Distribution
CPT-based					
$q_{c,GU1}$	MPa	7.9	3.0	0.37	Lognormal
$q_{c,GU2}$	MPa	19.2	7.5	0.39	Normal
$q_{c,GU3}$	MPa	11.1	6.1	0.54	Lognormal
$q_{c,GU4}$	MPa	1.8	0.4	0.22	Lognormal
$q_{c,GU5}$	MPa	36.3	12.3	0.33	Lognormal
$f_{s,GU1}$	kPa	39	20	0.51	Normal
$f_{s,GU2}$	kPa	115	46	0.39	Normal
$f_{s,GU3}$	kPa	103	33	0.32	Normal
$f_{s,GU4}$	kPa	50	30	0.60	Lognormal
$f_{s,GU5}$	kPa	177	93	0.52	Normal
Resistance					
$q_{c,pile,GU2}$	MPa	19.2	1.3	0.07	Normal
$q_{c,pile,GU3}$	MPa	11.1	1.4	0.13	Normal
$q_{c,pile,GU4}$	MPa	1.8	0.16	0.08	Normal
$q_{c,pile,GU5}$	MPa	31.4	1.0	0.03	Normal
$q_{c,filter}$	MPa	38.6	4.6	0.12	Normal
f_y	N/mm^2	485	48.5	0.10	Normal
Model factors					
θ_d	–	1.0	0.10	0.10	Normal
θ_F	–	1.0	0.10	0.10	Normal
θ_M	–	1.0	0.10	0.10	Normal
θ_N	–	1.0	0.10	0.10	Normal
θ_{Msf}	–	1.0	0.10	0.10	Normal
Load					
$Q_{surcharge}$	kPa	40.0	4.0	0.10	Normal

CPT's high measurement frequency with depth means it is far easier to statistically describe soil variability with depth and distance compared to discrete laboratory tests making it easier to model accurately.

A finite element reliability assessment of the quay wall was accomplished by coupling PLAXIS with the open-source reliability toolbox OpenTURNS (Baudin et al., 2015). Latin hypercube sampling (LHS) was used to generate CPT traces based on the underlying distributions measured at the site, see Table 1. The simulated CPT traces were then transformed using the relations in Table 2 into the required constitutive model parameters for the finite element model. Each CPT trace was

Table 2
CPT correlations and equations used in estimating the constitutive model parameters.

Parameter	Soil type	Correlation	Reference
Strength parameters			
Friction angle, φ'	Sand	$\varphi' = 17.6 + 11.1\log\left(\frac{q_c}{p_a}\right)/\left(\frac{p_a}{\sigma_{v0}}\right)^{0.5}$	Kulhawy and Mayne (1990)
	Clay	$\varphi' = 29.5B_q^{0.121}(0.256 + 0.336B_q + \log Q_m)$	Mayne (2005)
Cohesion, c'	Clay	$c = 0.03\sigma_{v0}'$	
Dilatancy angle, ψ	Sand	$\psi = -2 + 12.5D_r/100$	Brinkgreve et al. (2010)
Reference stiffness			
Tangent stiffness for primary oedometer loading, E_{oed}^{ref}	All	$E_{oed} = 5(q_t - \sigma_{v0})E_{oed}^{ref} = E_{oed}/\left(\frac{\sigma_{v0}'}{p_a}\right)^m$	Robertson (2009)
Secant stiffness in standard drained triaxial test, E_{50}^{ref}	Sand	$E_{50}^{ref} = E_{oed}^{ref}$	Brinkgreve, et al.(2010)
	Clay	$E_{50}^{ref} = 1.25E_{oed}^{ref}$	Schmudderich et al.(2020)
Unloading-reloading stiffness, E_{ur}^{ref}	Sand	$E_{ur}^{ref} = 3E_{oed}^{ref}$	Schmudderich et al.(2020)
	Clay	$E_{ur}^{ref} = 5E_{oed}^{ref}$	Schmudderich et al.(2020)
Power for stress-level dependency of stiffness, m	Sand	$m = 0.7 - D_r/320$	Brinkgreve et al. (2010)
	Clay	$m = 1.0$	Brinkgreve et al. (2010)
Small strain stiffness			
Initial shear modulus, G_0	All	$G_0 = \alpha q_t$	Lai et al. (2025)
Shear stain at $0.7G_0$, $\gamma_{0.7}$	All	$\gamma_{0.7} = 0.107G_0[2c(1+cos2\varphi) + \sigma_{v0}'(1+K_0)sin2\varphi$	Benz (2007)
State parameters			
Unit weight, γ	All	$\frac{\gamma}{\gamma_m} = 0.027\log R_f + 0.36\log\left(\frac{q_t}{p_a}\right) + 1.236$	Robertson and Cabal (2010)
Overconsolidation ratio, OCR	Sand	$OCR = 0.32(q_t - \sigma_{v0})^{0.72}/\sigma_{v0}'$	Agaiby and Mayne (2019)
	Clay	$OCR = 0.33(q_t - \sigma_{v0})/\sigma_{v0}'$	Robertson (2009)

treated deterministically within the finite element model, and the results were fed back to the reliability toolbox, where they were integrated together to form output distributions allowing for the calculation of reliability indices.

Prior to conducting the full analysis, a convergence study was performed to determine the required number of numerical realisations for reliable reliability index estimation. The results revealed that the reliability index stabilised after approximately 100 realisations, with subsequent fluctuations remaining below 1 %. Based on this convergence behaviour, a total of 250 numerical realisations were executed to ensure a robust reliability calculation.

3.1. Limit state functions of quay walls

Limit state functions (LSFs) mathematically define the threshold at which either the capacity is exceeded (i.e. the ultimate limit state, ULS) or excessive deformation occurs (serviceability limit state, SLS), denoted by $Z = 0$. Based on the limit state function, the reliability index β is defined by:

$$\beta = \frac{\mu_Z}{\sigma_Z} \tag{1}$$

where μ_z is the mean value of the limit state function and σ_z is the standard deviation of the limit state function. The simple moment method, see Equation (1), offers a practical and efficient approach for finite element-based reliability assessment compared with the First-Order Reliability Method (Rackwitz and Flessler, 1978) and Monte Carlo Simulation (Whitman, 1984). In FE analyses, the limit state function is implicit, and gradients are not readily available, making the First-Order Reliability Method difficult to apply without additional approximations, such as response surface approximation. Monte Carlo Simulation, while robust, is computationally prohibitive for large scale FE models. The moment method thus provides a reasonable compromise between accuracy and efficiency. Its main assumption is that the limit state can be represented by a normal distribution, which was verified to be reasonable for the numerical outputs in this study. This assumption is further supported by the law of central tendency, whereby the combined effect of numerous independent input uncertainties tends to yield an approximately normal response distribution, even when the individual variables themselves are non-normal.

The probability of failure p_f is inversely related to the reliability index, and is typically approximated using the standard normal cumulative distribution function of the reliability index (Phoon et al., 2022). According to both the Eurocode (NEN, 2017; van den Eijnden et al., 2024) and Dutch quay wall guidelines (de Gijt and Broeken, 2013), the target lifetime reliability index β_t of a quay wall is usually 3.8 (Roubos et al., 2021). This target corresponds to a consequence class CC2 where risk to human life is negligible yet economic damage is high.

This study considers five primary failure modes (Fig. 4), each with their own distinct limit state function Z. Four of these failure modes pertain to the ultimate state (ULS) and one pertaining to the serviceability limit state. The structural and geotechnical reliability of the screw injection piles underneath the relieving platform was not considered because of an infinitesimally small failure probability (where $\beta > 8$), beyond the computational capacity of OpenTURNs and the computer. A failure tree was used to combine the different failure modes. Each failure mode is assumed to be independent and therefore connected in series, i.e., the overall quay wall system is considered to fail once any single failure mode occurs. This representation provides a conservative reliability estimate (Pan and Jia, 2025).

3.1.1. Failure in front wall

Structural failure of the combined wall $Z_{wall,ULS}$ describes when the point at which the yield strength of the open-ended piles is exceeded:

$$Z_{wall,\,ULS} = f_y - \max\left(\frac{\theta_M M_{wall}(z)}{W_{wall}} + \frac{\theta_N N_{tube}(z)}{A_{tube}}\right) \tag{2}$$

where f_y is the yield strength of steel, M_{wall} is the bending moment in the combined wall, N_{tube} is the axial force on open-ended piles of the combined wall, W_{wall} is the section modulus of the combined wall and A_{tube} is the section area of the tube pile. θ_M and θ_N are factors accounting for the model uncertainty for the bending moment and axial force respectively.

Wall deformations are considered by the serviceability limit state $Z_{wall,SLS}$, whereby:

$$Z_{wall,\,SLS} = d_{wall,\,SLS} - \theta_d d_{wall,max} \tag{3}$$

$d_{wall,SLS}$ is the maximum allowable wall deformation for SLS, $d_{wall,\max}$ is the wall deformation at the point of maximum deformation and θ_d is a factor accounting for model uncertainty in the predicted wall deformations.

3.1.2. Failure in anchors and piles

The limit state functions of the anchor have been discretised into structural $Z_{anchor,str}$ and geotechnical limit states $Z_{geo,str}$ the minimum of

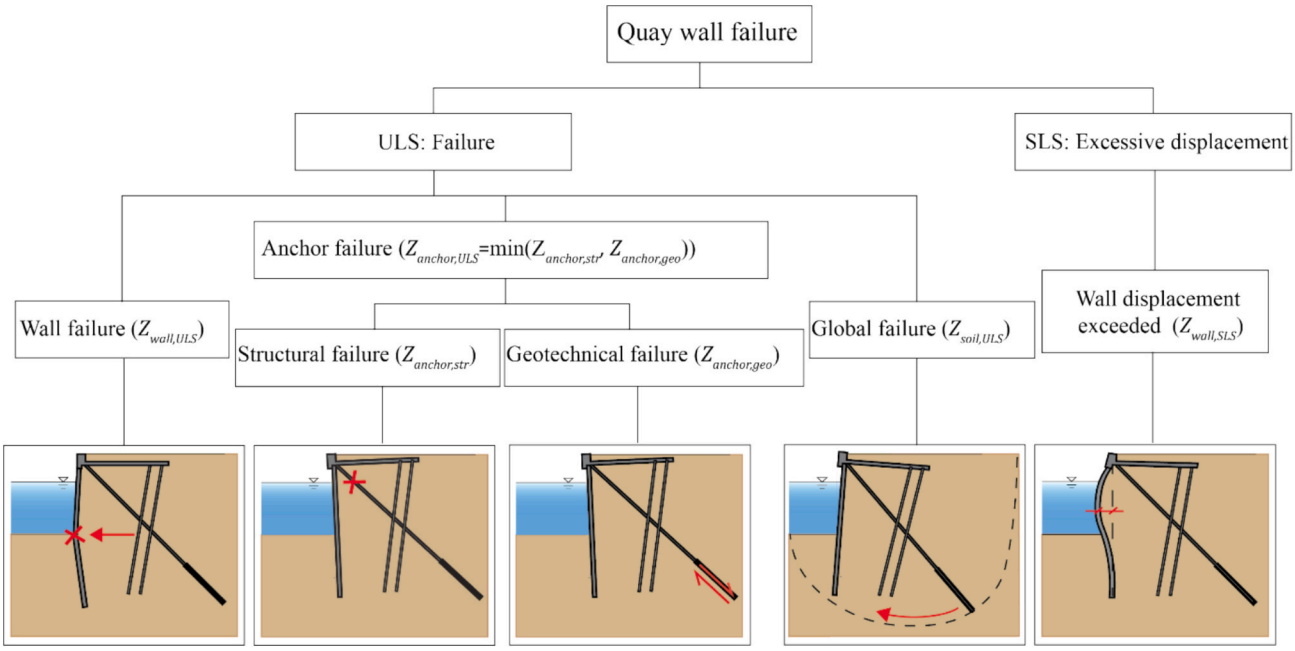

Fig. 4. Quay wall failure modes considered in this study.

which defines the ULS of the anchor $Z_{anchor,ULS}$:

$$Z_{anchor,\,str} = f_y - \frac{\theta_F F_{anchor}}{A_{anchor}} \tag{4}$$

$$Z_{anchor,\,geo} = R_{anchor} - \theta_F F_{anchor} \tag{5}$$

$$Z_{anchor,\,ULS} = \min(Z_{anchor,\,str}, Z_{anchor,\,geo}) \tag{6}$$

where f_y is the yield strength of the anchor, F_{anchor} is the actual anchor force, R_{anchor} is the geotechnical capacity of the anchor, and θ_F is a factor that introduces model uncertainty in predicting the anchor force. The same formulation can be applied to the compression piles, using the compressive strength f_c and geotechnical capacity of the pile R_{pile} to get the limit states $Z_{pile,str}$ and $Z_{pile,geo}$ respectively.

3.1.3. Failure in global stability

Global instability can also occur across the entire quay wall through either failure of the passive soil wedge or rotational failure of the entire quay structure (de Gijt and Broeken, 2013; Roubos et al., 2018). In finite element modelling, global instability is often represented by the global safety ratio ΣMsf, steadily reducing the friction angle φ' and cohesion c' until geotechnical failure occurs—thus referred to as φ-c reduction or shear strength reduction). The ultimate limit state for global stability $Z_{soil,ULS}$ can therefore be represented by:

$$Z_{soil,ULS} = \theta_{Msf} \sum Msf - 1 \tag{7}$$

where θ_{Msf} is the model uncertainty factor.

3.2. Finite element model

The FE model was developed using Plaxis 2D. To capture the complex soil stress paths during construction, the hardening soil with small-strain stiffness (HSS) constitutive model (Brinkgreve, 2005) was used. HSS simulates the combined effects of excavation-induced unloading and deviatoric loading through its friction and cap hardening mechanisms. The model requires ten primary input parameters: the strength parameters (friction angle φ, cohesion c and dilatancy angle ψ), the reference stiffness parameters (secant stiffness in standard drained triaxial test E_{50}^{ref}, tangent stiffness for primary oedometer loading E_{oed}^{ref} and unloading–reloading stiffness E_{ur}^{ref}, and power for stress-level dependency of stiffness m), the small strain parameters (initial shear modulus G_0 and the shear stain $\gamma_{0.7}$ at $0.7G_0$) and the state parameters (unit weight γ and over consolidation ratio OCR).

The combined wall, front wall and relieving platform were all modelled using plate elements with a linear-elastic constitutive model. The connection between the wall was modelled as a hinge (Lai et al., 2025).

To model three-dimensional effects in a two-dimensional space, the MV anchors and SI piles were modelled as an embedded pile row, a feature in Plaxis 2D which models pile rows by superimposing a Mindlin beam element onto the mesh, with a special out-of-plane interface to connect the beam with the soil nodes, representing the pile-soil interaction (Sluis et al., 2014). Lastly, to relate the soil strength to the interface adhesion and material roughness, all structural members used a strength reduction factor R_{inter} of 0.8 (de Gijt and Broeken, 2013; Han et al., 2018).

3.3. Statistical characterisation of input variables

In this study, uncertainties in CPT parameters, applied loads, material properties and models were accounted for, as shown in Table 1. These uncertainties are categorised into two types: parametric uncertainty and model uncertainty. Parametric uncertainty reflects inherent material variability that limits the determinability of key design parameters. This uncertainty is particularly significant in soil where the spatial and temporal variability of properties can be quite large stemming from fabric anisotropy and the soils' depositional and stress histories. Parametric uncertainty also affects geometrical dimensions, structural material properties, and applied loads through construction tolerances and operational fluctuations. It can be conservatively accounted for using point statistics (e.g. mean and standard deviation) or it can be more accurately described using stochastic random fields that spatially constrain soil variability. Since the two-dimensional FE model used in this study requires homogeneous layers in each simulation, all soil parameters, geometric tolerances, material strengths, and load levels were characterised by point statistics (Table 1).

3.3.1. CPT-based input parameters

For each numerical realisation, a set of CPT values was sampled from the measured q_c distributions of each Ground Unit (Table 1 and Fig. 5). These values were then correlated to HSS model parameters using the correlations outlined in Table 2. The adopted correlations were calibrated and validated against laboratory data using Plaxis SoilTest. The calibrated numerical responses, obtained through CPT-based correlations, showed good agreement with results from triaxial and oedometer tests on site samples in the Port of Rotterdam, confirming the reliability of the adopted correlation. Further details of the calibration and validation procedures are provided in Lai et al. (2025).

To determine the geotechnical capacity of the screw injection piles, the following equation was used:

$$R_{pile} = \alpha_p q_{c,filter} A_{base} + O_{pile} \sum_{i=1}^{n} \alpha_s q_{c,avg,i} L_i \tag{8}$$

where α_p and α_s are correlation factors for the base and shaft resistance respectively, $q_{c,filter}$ is a weighted average of cone resistances around the pile tip determined using the filter method by Boulanger and DeJong (2018), A_{base} is area of the pile base, O_{pile} is the circumference of the pile based on its outermost diameter (=850 mm), $q_{c,avg,i}$ is the average cone resistance across Ground Unit i, L_i is the length of the pile in Ground Unit i, and n is the number of ground units (five in this case).

Similarly, the geotechnical capacity of the MV anchors was estimated using:

$$R_{anchor} = O_{anchor} \sum_{i=1}^{n} \alpha_t q_{c,avg,i} L_i \tag{9}$$

where α_t is a correlation factor for the tensile resistance of the anchor and O_{anchor} is the surface area of the pile shaft (2.67 m^2 and 2.32 m^2 for the SI piles and MV anchors respectively).

The factors α_p, α_s and α_t depend on the installation and soil type. Extensive tests across the Port of Rotterdam have been performed over recent years to understand the geotechnical capacity of the piles (Duffy et al., 2024b; Matic et al., 2019; Putteman et al., 2019; Spruit et al., 2022). Based on these tests, an α_p of 0.30 and an α_s of 0.012 have been used for the screw injection piles and an α_t of 0.0125 for the MV anchors.

3.3.2. Spatial averaging

In this study, a 2D FE model with homogeneous layers was used, which means that an "effective input property" needs to be defined for each layer—a property which represents the mobilised shear strength across the length of the failure surface (Ching et al., 2016; Griffiths et al., 2012; Hicks and Samy, 2002). For limit states governed by weak zones like the global slip failure $Z_{soil,ULS}$, the tendency for such failure mechanisms to seek out weak zones means that the failure surface is difficult to anticipate beforehand without more computationally intense finite element models (Tabarroki et al., 2022; van den Eijnden et al., 2024).

Spatial averaging was only accounted for in the geotechnical failure of anchors or piles considering the anchor and pile shaft resistance, which relies heavily on the averaged soil properties along the entire embedded length of anchors and piles, instead of thin local weak zones. This averaging provides a realistic representation of the mobilised soil behaviour (Liu et al., 2015; Tabarroki et al., 2022). In contrast, the pile base resistance was not spatially averaged because it is controlled by a limited soil zone beneath the tip, where a local weak layer can dominate the response. For the screw injection piles considered here, the base contribution to total capacity is relatively small, so any weak layer near the base has minimal influence on overall performance.

Therefore, to model the shaft resistance of the anchors and piles, 10,000 random field realisations of q_c along the anchor length were performed, with the vertical scale of fluctuation derived from CPTs across the site. The average q_c from these realisations were then used as the input to Equation (9), from which the anchor capacity could be derived. This resulted in a comparable mean capacity (Fig. 6) to the original distribution, albeit with considerably less variation. Further details of the calculation procedures are provided in Hao et al. (2025).

3.3.3. Modelling uncertainty

Model uncertainty reflects the model's ability to represent reality, that is, the deviation between the measured and predicted response. For

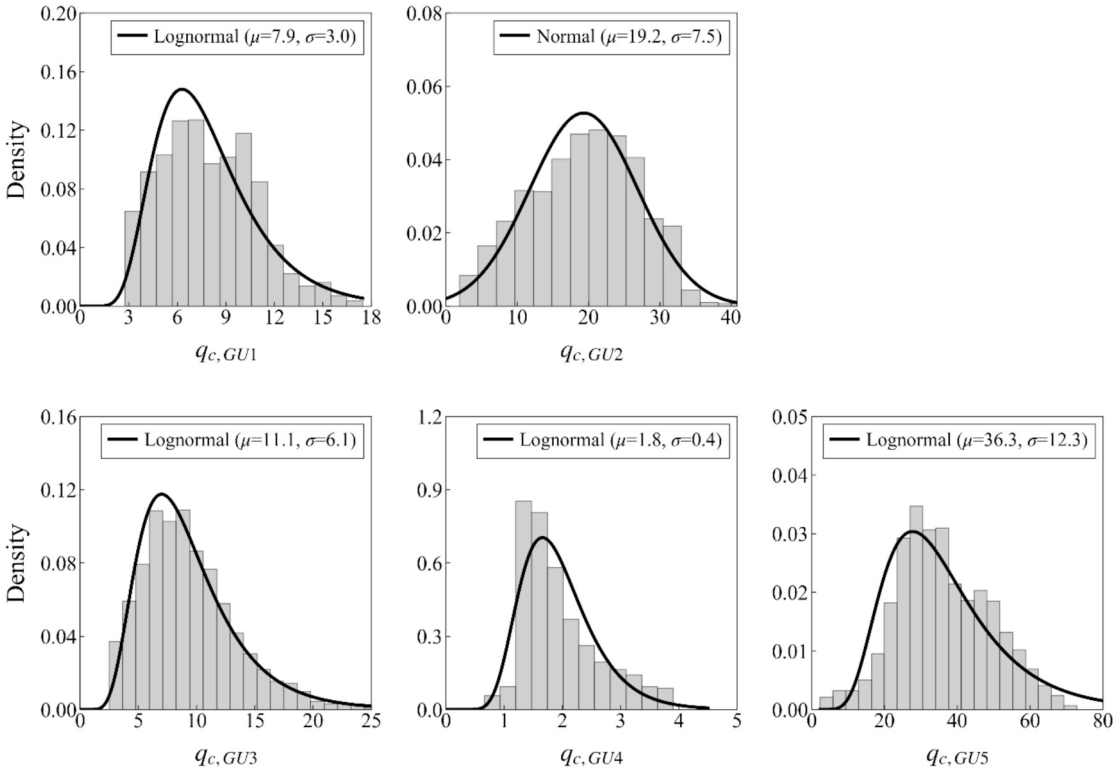

Fig. 5. Histogram of CPT parameters in different soil units.

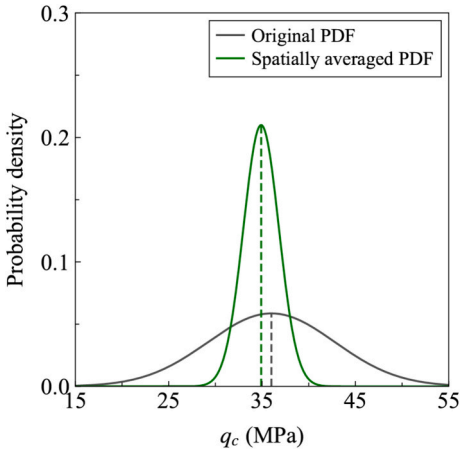

Fig. 6. Influence of spatial averaging on the input q_c value for the anchor capacity.

the quay wall, the model uncertainty for each limit state function is represented by the stochastic model factors θ_d, θ_F, θ_M, θ_{Msf} and θ_N, which describe the difference between the numerical model and reality. However, calibrating these factors with any sort of certainty requires an extensive set of component-specific tests and full-scale test on the quay wall itself. For this reason, the expected value of the model factors have been set to 1.0 with a coefficient of variation of 0.1—in line with general recommendations from literature (van den Eijnden et al., 2024) and for quay walls (Roubos et al., 2021).

4. Results

4.1. Validation with construction data

Comparison of the measured wall deformations and anchor forces with predictions of the 250 numerical simulations are shown in Fig. 7 and Table 3. In Fig. 7a and Fig. 7b, these comparisons are made at the end of dredging phase 2 and phase 4, where the seabed reached depths of − 16 m and − 24.5 m respectively. The measured deformations fall within the realisations of the finite element model (Fig. 7b), with the point of maximum deformation aligning close to the average deformation across all realisations, with a mean absolute error (MAE) of 2.6 mm (≈7 %). This comparison increases confidence in the calculated reliability of the serviceability limit state, which is governed by the maximum wall deformation located at the combined wall.

Table 3
Comparison of the numerical results to the measurements, including the Mean Absolute Error (MAE), the Root Mean Squared Error (RMSE) and the coefficient of determination R^2.

Measurement		MAE	RMSE	R^2
Wall deformation after Phase 4	Maximum point	2.6 mm	5.8 mm	0.76
	Top point	10.3 mm		
Anchor force		143 kN	173 kN	0.68

The only exception is near the top of the wall, both above and near the interface between the concrete superstructure and the steel combined wall where deformations are overestimated by all realisations. This effect is likely a result of three-dimensional effects in the quay wall. In the out-of-plane direction, the wall consists of two distinct sections: a 23 m cast in-situ concrete superstructure and a 3.3 m combined wall connected by interlocks. The deformation of the concrete superstructure with higher lateral stiffness is strongly influenced by adjacent concrete blocks, which cannot be captured in a 2D analysis. In particular, the simulated location lies fifty metres away from a stretch of the quay wall where the dredged depth is four metres higher, resulting in less deformation predicted in the 2D model across this section. A full 3D analysis could better capture the out-of-plane stiffness of the concrete superstructure and the effects of non-uniform dredging, thereby improving the accuracy of predicted wall deformations, albeit at a substantially higher computational cost.

In addition, since the anchor is directly connected to the front wall of the superstructure, changes in the tensile force on the anchor are inherently correlated with the measured deformations in the front wall. The calculated wall deformations are slightly higher than the measured deformations, and therefore the anchor loads in some dredging phases (Fig. 7c) tend to be slightly overestimated in some numerical realisations, leading a slightly high calculated reliability index. Nevertheless, the measured anchor forces fall within the range of most of the realisations, with an MAE of 143 kN across all dredging phases (15 % of the measured anchor force). The measured and predicted forces are substantially lower than the design capacity of 7000 kN. This is partly because no surcharge loading was present at the end of construction, but also because the anchors are generally conservatively designed to account for the potential influence of soil movement within the global slip failure plane on the anchor's tensile capacity.

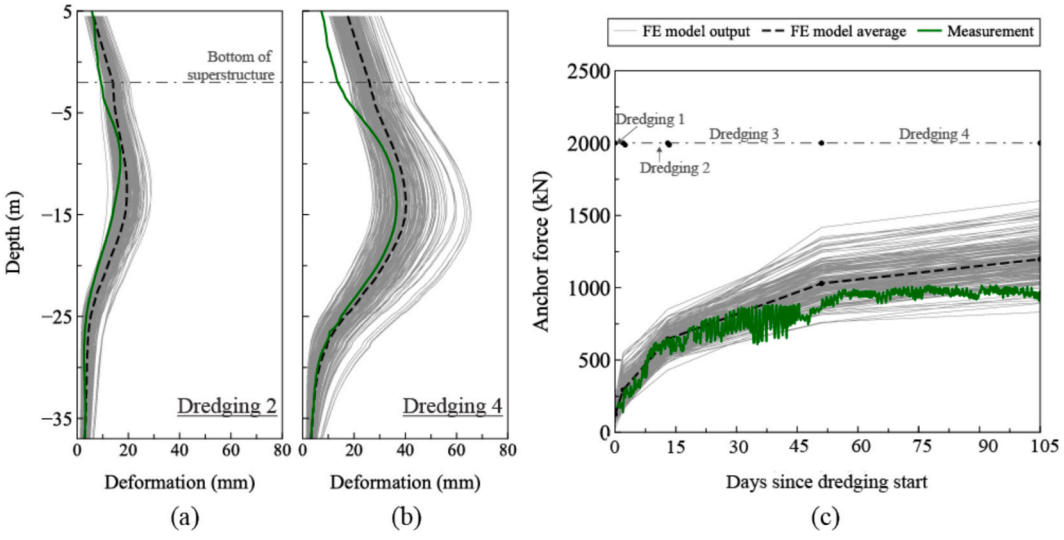

Fig. 7. Comparison between the measured and numerical results from all realisations: (a) and (b) wall deformation during Phase 2 and 4; (c) anchor force evolution over time.

Validation in this study was limited to wall deformations and anchor forces, as these were the only parameters consistently monitored during staged dredging. Other quantities such as bending moments, pore pressures, and pile base reactions were unavailable, and no data exist under operational surcharges since the quay has not yet entered service. Consequently, the framework was validated only against short-term construction data, without capturing long-term processes such as settlement, cyclic loading, corrosion, or material degradation. This limitation should be borne in mind, and future applications should integrate broader monitoring datasets and time dependent effects to improve lifecycle reliability assessments.

4.2. Current failure probability

Beyond just the measured properties, the 250 numerical realisations enable a systematic uncertainty quantification of the model responses. The resulting distributions of key outputs, including wall's bending moment, wall's axial force, anchor force, global stability ratio, and lateral wall deformation, are summarised in Fig. 8. These distributions reflect the propagation of both parametric uncertainty and model uncertainty into the structural and geotechnical responses. All the outputs follow approximately normal distributions. This maximum wall deformation exhibits the highest coefficient of variation of 19.2 %, indicating that the serviceability response is most sensitive to the input uncertainties. For all other limit states, the CoV varies from 2.1 % to 8.4 %.

Building on these quantified uncertainties, the reliability indices of the five limit states were derived by combining the model outputs with Equation (1) and comparing them with the target reliability index β_t of 3.8. As shown by Fig. 9, all reliability indices are above 3.8, showing that quay wall meets the safety requirements. The structural stability of the wall $Z_{wall,ULS}$ shows the lowest reliability index of 4.3, indicating the least safety margin. This compares well with the study by Roubos et al., (2021). The lowest reliability index since the average demand was close to the yield strength of the combined wall in spite of the low CoV of bending moment and axial force. Compared with other modes, wall failure offers easier detection through installing sensors into the wall and monitoring for forces and movements. Meanwhile, the global safety ratio $Z_{soil,ULS}$ also showed negligible safety margin with a reliability index of 4.6. This observation implies that simple structural

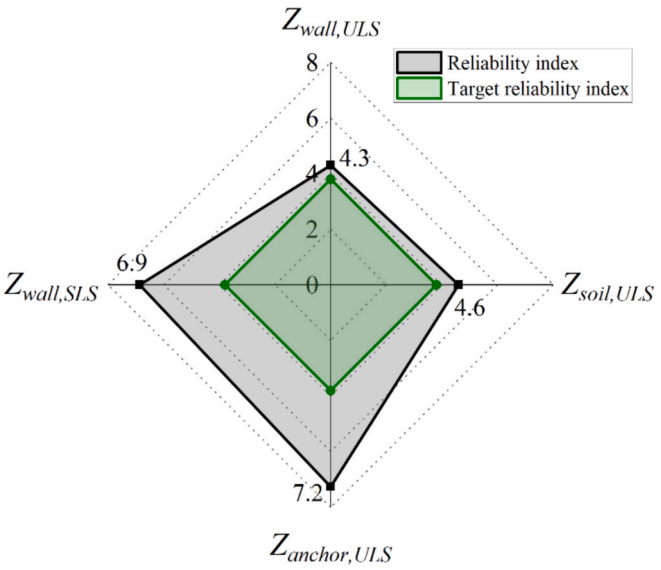

Fig. 9. Reliability indices for different limit state functions.

reinforcement is not sufficient, as soil landslides could occur despite sound structural conditions. Future wall improvements must therefore consider both the structural and soil response in tandem.

While the maximum wall deformation $Z_{wall,SLS}$ showed the highest CoV across all modelling realisations, conversely, its reliability index of 6.9 was well above β_{target}, since the allowable wall deformation for SLS conditions (1)% of the height of retaining wall = 275 mm) was well above the average wall deformation (62.9 mm) predicted by the finite element model. Similarly, the reliability of $Z_{anchor,ULS}$ was above β_t since the anchors are generally conservatively designed to account for any interaction effects between the active zone behind the quay wall and the anchor itself, as well as failure in adjacent anchors.

It should be mentioned that in this study, the soil profile was simplified as homogeneous layers, thereby neglecting intra-layer variability such as clay lenses, which may mask weak zones and lead to an overestimation of reliability (Fenton et al., 2005; Hicks and Spencer,

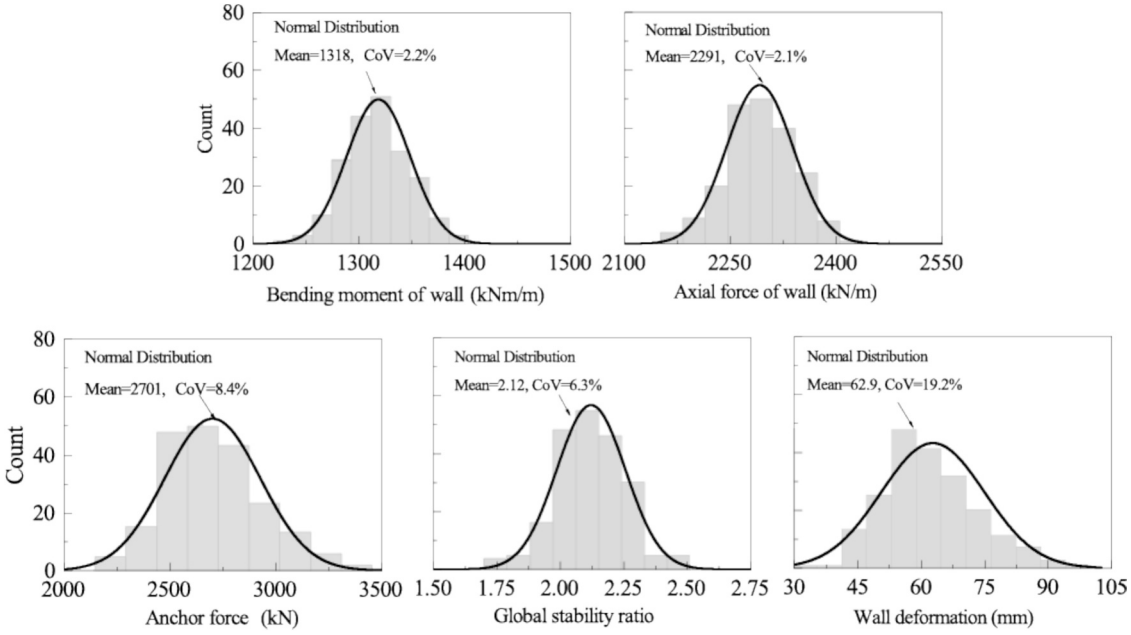

Fig. 8. Histograms of numerical results: (a) bending moment of wall (b) axial force of wall (c) anchor force (d) global stability ratio and (e) maximum wall deformation.

2010). Future work should therefore apply random finite element methods to better capture intra-layer heterogeneity and support robust life-cycle reliability assessments.

4.3. Influence of spatial averaging

To show the influence of spatial averaging on the reliability of the anchors and piles, two different methods for deriving the input q_c distribution were examined: one by spatial averaging $q_{c,avg}$ and the other derived from the original distribution of CPT cone resistances (Fig. 6). While the mean of the spatially averaged distribution was slightly lower compared to the original distribution, the variance was also much lower than that of the original distribution. Consequently, the resulting reliability index was much higher for the spatially averaged situation (Fig. 10), almost twice as high for both the MV anchors and SI piles. These reliability indices also reflect observations from both the on-site measurements and pile tests performed at the site—which have not indicated any significant failures or deformations at any of the piles.

5. Sensitivity analysis

During a quay wall's service life, port authorities or terminals seek to enhance a quay wall's functionality to accommodate for evolving operational demands. Typical modifications may include deepening of the seabed level in front of the wall to accommodate bigger vessels, or increasing the operational loads behind the quay wall (Bauduin et al., 2017; Roubos et al., 2021; Ruggeri et al., 2019). It is of interest therefore to establish the sensitivity of the reliability indices to changes in both dredge level and surcharge loading. As part of this study, time-dependent effects which include corrosion of the front wall (Hu and Luo, 2018; Osório et al., 2010; Roubos et al., 2020; Ruggeri et al., 2019) as well as the effect of variable loads created from changing surcharge loads or changing water levels in front of or behind the quay wall were not considered.

5.1. Influence of surcharge loads

Surcharge loading behind a quay wall comes from various sources, including live loads from passing traffic, gantry cranes and temporary storage, as well as permanent loads such as embankments and fixed infrastructure. Correspondingly, surcharge loading is one of the key parameters when examining a quay wall's remaining lifetime or its suitability for repurposing (Bauduin et al., 2017). For example, surcharge loading outside of normal traffic zones may reach up to 60 kPa for container or ro-ro terminals (EAU, 2012; Ruggeri et al., 2019), and up to 150 kPa in the case of ore-handling terminals (de Gijt and Broeken, 2013). In this study, the influence of uniform surcharge load was studied, reflecting the design configuration of pipelines and tanks. In other quay wall configurations with highly localized live loads, such as crane loads, the assumption of a concentrated surcharge should be adopted, as the resulting additional bending moments may have a different impact on the reliability indices.

Operational surcharge loading of the quay wall was set to 40 kPa. Unsurprisingly, increasing the surcharge load from this point results in a reduction of reliability indices (Fig. 11), reducing below the target reliability index once the surcharge load exceeds 80 kPa. The increase in active earth pressures results in the most dangours failure modes being the structural failure in the wall $Z_{wall,ULS}$. In contrast, the anchor stability $Z_{anchor,ULS}$ is quite stable, likely because of the alleviating influence of the relieving platform on the rotation of the superstructure. Therefore, exceeding the surcharge limit of 80 kPa would require significant structural reinforcement, or reduction of dredged depth.

To further examine the trends in the reliability indices, Fig. 12 shows the distributions of the numerical results. In these analyses the dredge level in front of the wall is fixed at −24.5 m. For each failure mode except the soil failure considered, the numerical output falls and the COV rises as the surcharge pressure increases from 40 kPa to 120 kPa. Therefore, the reliability index reduces. For soil failure, the allowable safety factor represents the minimum acceptable limit. Consequently, a decrease in both the mean and standard deviation of the calculated safety factor further diminished the LSF output, resulting in lower reliability. As surcharge pressure rises, both the mean of the wall's bending moment and axial force increase significantly. Yet compared to the other limit states, the coefficient of variation in the results is relatively small, essentially reflecting the uncertainty around the derived reliability indices. In contrast, while $Z_{wall,SLS}$ does not reduce below the target reliability index, its reliability index decreases the fastest over time because its CoV decreases the most from 19.3 % to 20.4 % and shows the highest variation in terms of the maximum predicted deformations. The relieving platform likely alleviates a significant amount of lateral deformation at the front wall, yet the results also show the importance of proactive instrumentation procedures in obtaining early warning signs of excessive deformation (like the inclinometers installed along the quay wall).

5.2. Influence of dredge level

The dredge level or seabed depth in front of the wall is a critical design and operational consideration, as it governs the guaranteed nautical depth required to safely accommodate larger vessel keels. As

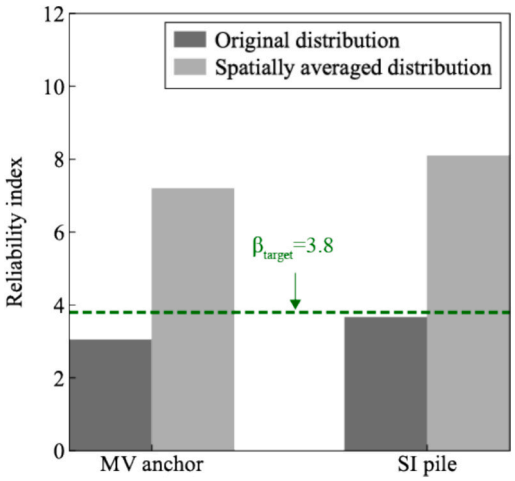

Fig. 10. Influence of input distribution on reliability indices.

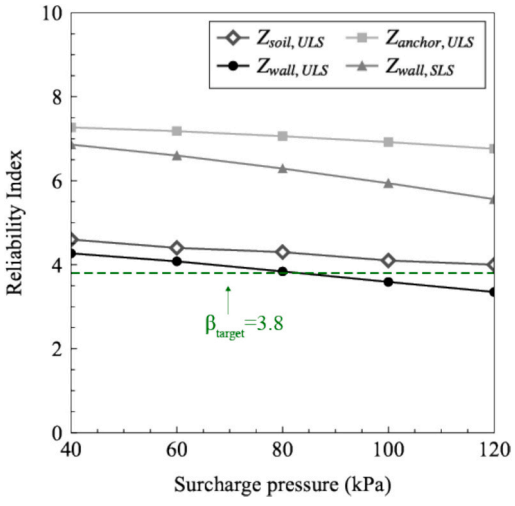

Fig. 11. Influence of increasing surface loads on reliability indices of the quay wall.

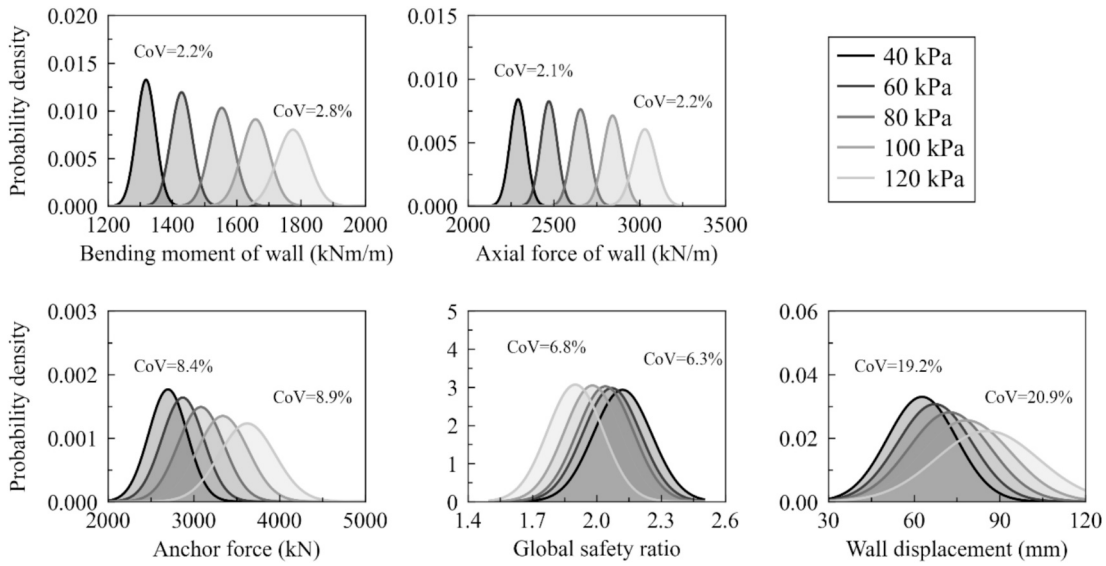

Fig. 12. Probability density function of numerical results in different surcharge loads.

ports compete for capacity and seek to attract larger vessels, periodic or permanent deepening of berth areas is becoming increasingly common (Sihombing et al., 2025). The seabed depth may also change due to natural influence, including sedimentation (Buisman et al., 2024) and scouring (Ferraro et al., 2024; Roubos et al., 2014; Yuksel et al., 2019). In either case, seabed deepening highly influences quay wall performance and constitutes a key aspect of port asset management.

Considering reductions in dredge level from the current operational level of − 24.5 m (Fig. 13), all reliability indices decrease due to the decrease passive earth pressure but are still above 3.8. Owing to the depth of the base of the sheet piles of −28.5 m, this study does not analyse the reliability indices below −27.5 m. The structural failure in the wall $Z_{wall,ULS}$ is again the governing limit state.

Just like what is observed with the variations in surcharge load, the serviceability limit state for the retaining wall $Z_{wall,SLS}$ is particularly sensitive to changes in dredge level, decreasing rapidly with increase in berth depth. This is because of the non-linear increase in bending moment as the effective span of the wall increases. Notably, the wall deformation also has the highest uncertainty amongst all limit states (Fig. 14), increasing in CoV from 19.2 % to 20.9 % with deeper dredged depths.

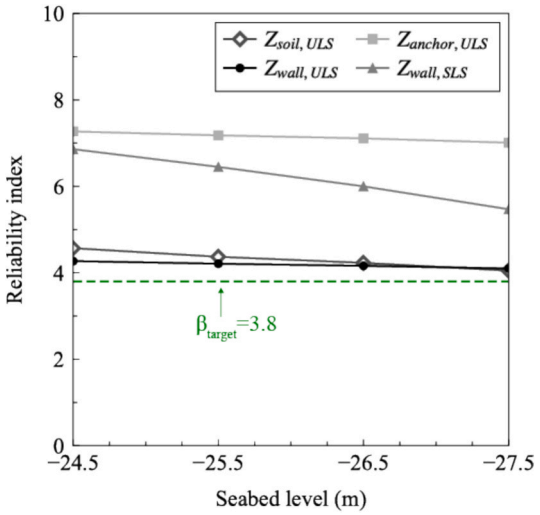

Fig. 13. Influence of berth deepening on the quay wall's reliability indices.

Figs. 11 and 13 show that wall deformations, bending moments, and anchor forces increase, while the global safety ratio decreases, with increasing dredging depth and surcharge loading. These trends are explained by higher active earth pressures associated with deeper dredging and reduced passive resistance under larger surcharges, both of which reduce the reliability indices and push the quay wall closer to unsafe conditions. Across these scenarios, structural failure of the wall consistently remains the governing failure mode, while the serviceability limit state ($Z_{wall,SLS}$) is the most sensitive, showing the steepest decline in reliability indices due to variability in wall deformations. In contrast, anchor stability remains relatively robust, partly due to the influence of the relieving platform. Overall, these findings indicate that hypothetical operational changes may primarily affect the wall's structural and serviceability limit states, underscoring the need for targeted monitoring and reinforcement strategies.

6. Conclusion

This study has presented a CPT-based finite element reliability-based framework for assessing the performance of quay walls, validated against detailed field measurements from an instrumented quay wall in the Port of Rotterdam. Unlike most existing approaches that rely on simplified analytical models, a limited number of failure modes, or empirical parameter correlations, the proposed framework integrates performance-based reliability analysis with field consistent CPT data to directly capture site-specific variability. It directly samples from distributions of measured CPT parameters, thus improving the computational efficiency by reducing the size of each sample set whilst providing a well-characterised input distribution for each parameter across the quay wall section in question. The set of CPT parameters were correlated directly to constitutive model parameters, creating realistic parameter combinations without relying on site-specific correlation coefficients.

The calculated reliability indices indicates that wall failure emerged as the most critical mode, aligning with Roubos et al. 2021, while wall deformation showed the highest uncertainty, warranting continued monitoring.

The study also highlighted the influence of spatial averaging on the performance of the tension anchors. Spatial averaging of CPT input parameters was found to significantly increase the reliability of tension anchors, aligning with observations for field measurements. The tension anchors are also affected by the deformation of stiff concrete superstructure, owing to directly connected. This will also change the reliability indices of anchor failure but not that of serviceability limit state

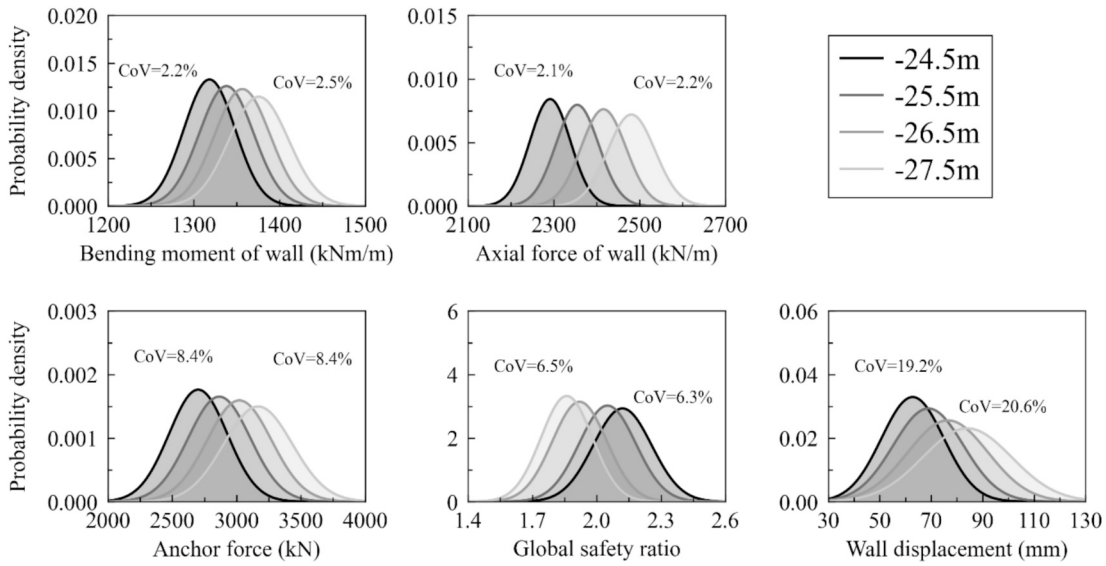

Fig. 14. Probability density function of numerical results in different seabed levels.

since this failure depends on the maximum wall deformation, typically occurring along the combined wall.

Sensitivity analyses further revealed that increased surcharge loads and deeper dredging reduce reliability of all failure modes. The structural failure of the wall is consistently the governing limit state across these different hypothetical scenarios, with changing surcharge loads generally causing a more rapid reduction due to its stronger effect on wall bending moments. Wall deformations showed the highest uncertainty, indicating that serviceability limit states are particularly sensitive to hypothetical changes such as dredging or increased surcharge loading.

This research proposed a performance-based reliability assessment, using the CPT-based constitutive parameters to avoid reliance on site specific parameter correlations. Although demonstrated for a quay wall in Rotterdam, the framework can be transferred to other sites by recalibrating CPT correlations though lab tests, adjusting the finite element model to local conditions, and incorporating region specific hazards such as seismic loading or liquefaction. Future research can build upon this work in several directions: (1) incorporating long-term monitoring datasets and explicitly modelling time-dependent deterioration processes such as corrosion, cyclic degradation, and creep; (2) representing intra-layer soil variability through random field approaches to better capture weak zones; (3) extending the methodology to 3D analyses to capture the influence of the stiff concrete superstructure and uniform dredging conditions on wall deformation and calculated reliability indices.

Data availability statement

The monitoring data presented in this study is the property of the Port of Rotterdam, other data is publicly available. Please contact the corresponding author with reasonable requests for data.

CRediT authorship contribution statement

Na Hao: Writing – original draft, Visualization, Software, Methodology. **Kevin Duffy:** Writing – review & editing, Visualization, Software, Resources. **Cormac Reale:** Writing – review & editing, Methodology. **Kenneth Gavin:** Writing – review & editing, Supervision, Methodology.

Declaration of competing interest

The authors declare the following financial interests/personal relationships which may be considered as potential competing interests: Na Hao reports financial support was provided by China Scholarship Council. Kenneth Gavin reports financial support was provided by EU Clarion Project. If there are other authors, they declare that they have no known competing financial interests or personal relationships that could have appeared to influence the work reported in this paper.

Acknowledgments

The first author acknowledges the support of the China Scholarship Council (CSC) and the Geo-Engineering Section of Delft University of Technology, The Netherlands. The last author acknowledges the support of the EU Clarion Project, Grant agreement ID: 101147041. In addition, support of the Port of Rotterdam is also greatly appreciated.

Data availability

Data will be made available on request.

References

Agaiby, S.S., Mayne, P.W., 2019. CPT evaluation of yield stress profiles in soils. J. Geotech. Geoenvironmental Eng. 145 (12), 04019104. https://doi.org/10.1061/(ASCE)GT.1943-5606.0002164.

Alesiani, P., Ruggeri, P., 2024. Assessment of load Test results on a Sheet Pile Quay Wall: the potential of 3D Numerical Modeling. J. Geotech. Geoenvironmental Eng. 150, 05024007. https://doi.org/10.1061/JGGEFK.GTENG-12368.

Armstrong, J., Helm, P., Preston, J., Loveridge, F., 2024. Economics of geotechnical asset deterioration, maintenance and renewal. Transp. Geotech. 45, 101185. https://doi.org/10.1016/j.trgeo.2024.101185.

Baudin, M., Dutfoy, A., Iooss, B., Popelin, A.-L., 2015. Open TURNS: An industrial software for uncertainty quantification in simulation. pp. 1–38. doi: 10.1007/978-3-319-11259-6_64-1.

Bauduin, C., Mengeot, P., Ganne, P., 2017. Design and construction issues for deepening and strengthening of existing quay walls, in: Proc. 19th International Conference on Soil Mechanics and Geotechnical Engineering. Presented at the 19th International Conference on Soil Mechanics and Geotechnical Engineering (ICSMGE17), International Society for Soil Mechanics and Geotechnical Engineering (ISSMGE), Seoul, South Korea, pp. 1811–1814.

Benz, T., 2007. Small-strain stiffness of soils and its numerical consequences. University of Stuttgart, Stuttgart, Germany. PhD Thesis.

Bokhoven, W., 1966. Recent quay wall construction at Rotterdam harbour. Proc. Inst. Civ. Eng. 35, 593–613. https://doi.org/10.1680/iicep.1966.8602.

Boulanger, R.W., DeJong, J.T., 2018. Inverse filtering procedure to correct cone penetration data for thin-layer and transition effects, in: Proceedings of the 4th International Symposium on Cone Penetration Testing (CPT'18). Presented at the Cone Penetration Testing 2018, CRC Press, pp. 24–44.

Brinkgreve, R.B.J., 2005. Selection of soil models and parameters for geotechnical engineering application, in: Soil Constitutive Models: Evaluation, Selection, and

Calibration. Presented at the GeoFrontiers 2005, ASCE, Austin, Texas, USA, pp. 69–98. doi: 10.1061/40771(169)4.
Brinkgreve, R.B.J., Engin, E., Engin, H.K., 2010. Validation of empirical formulas to derive model parameters for sands. Numer. Meth. Geotech. Eng. 137, 142.
Buisman, M., Draganov, D., Kirichek, A., 2024. Near real-time nautical depth mapping via horizontal optical fibers and distributed acoustic sensing. J. Appl. Geophys. 225, 105377. https://doi.org/10.1016/j.jappgeo.2024.105377.
Ching, J., Hu, Y.G., Phoon, K.-K., 2016. On characterizing spatially variable soil shear strength using spatial average. Probabilistic Eng. Mech. 45, 31–43. https://doi.org/10.1016/j.probengmech.2016.02.006.
de Gast, T., Hicks, M.A., van den Eijnden, A.P., Vardon, P.J., 2021. On the reliability assessment of a controlled dyke failure. Géotechnique 71, 1028–1043. https://doi.org/10.1680/jgeot.19.SiP.003.
de Gijt, J.G., Broeken, M.L., 2013. Quay Walls, 2nd, Edition. ed. CRC Press, Leiden, The Netherlands.
Duffy, K.J., Gavin, K.G., de Lange, D.A., Korff, M., 2024a. Base resistance of screw displacement piles in sand. J. Geotech. Geoenvironmental Eng. 150, 04024070. https://doi.org/10.1061/JGGEFK/GTENG-12340.
Duffy, K.J., Gavin, K.G., Korff, M., de Lange, D.A., Roubos, A.A., 2024b. Influence of installation method on the axial capacity of piles in very dense sand. J. Geotech. Geoenvironmental Eng. 150. https://doi.org/10.1061/JGGEFK/GTENG-12026.
EAU, 2012. Recommendations of the "Committee for Waterfront Structures Harbours and Waterways," 9th (Translation of the 11th German Edition). ed. Ernst & Sohn.
Ene, A., Schweckendiek, T., Popa, H., 2021. Probabilistic FEM-Analysis for the Retaining Wall of a Deep Excavation at SLS. In: Matos, J.C., Lourenço, P.B., Oliveira, D.V., Branco, J., Proske, D., Silva, R.A., Sousa, H.S. (Eds.), 18th International Probabilistic Workshop. Springer International Publishing, Cham, pp. 577–590. https://doi.org/10.1007/978-3-030-73616-3_44.
Fenton, G.A., Griffiths, D.V., Williams, M.B., 2005. Reliability of traditional retaining wall design. Geotechnique 55 (1), 55–62. https://doi.org/10.1680/geot.2005.55.1.55.
Feremans, G., Vanhooydonck, R., 2019. Full scale load test on historic quay wall in Antwerp, in: Proceedings of the 17th European Conference on Soil Mechanics and Geotechnical Engineering. Presented at the ECSMGE-2019, Icelandic Geotechnical Society (IGS), Reykjavik, Iceland. doi: 10.32075/17ECSMGE-2019-0374.
Ferraro, D., Lauria, A., Penna, N., Gaudio, R., 2024. Propeller scour phenomenon in the presence of a quay-wall and currents. Ocean Eng. 313, 119389. https://doi.org/10.1016/j.oceaneng.2024.119389.
Ge, J., Zhu, M., Sha, M., Notteboom, T., Shi, W., Wang, X., 2021. Towards 25,000 TEU vessels? a comparative economic analysis of ultra-large containership sizes under different market and operational conditions. Marit. Econ. Logist. 23, 587–614. https://doi.org/10.1057/s41278-019-00136-4.
Griffiths, D.V., Paiboon, J., Huang, J., Fenton, G.A., 2012. Homogenization of geomaterials containing voids by random fields and finite elements. Int. J. Solids Struct. 49, 2006–2014. https://doi.org/10.1016/j.ijsolstr.2012.04.006.
Han, F., Ganju, E., Salgado, R., Prezzi, M., 2018. Effects of interface roughness, particle geometry, and gradation on the sand–steel interface friction angle. J. Geotech. Geoenvironmental Eng. 144, 04018096. https://doi.org/10.1061/(ASCE)GT.1943-5606.0001990.
Hao, N., Li, X., Li, Y., Jia, J., Gao, L., 2022. A novel reliability-based method of calibrating safety factor: application to the cemented sand and gravel dams. Eng. Geol. 306, 106719. https://doi.org/10.1016/j.enggeo.2022.106719.
Hao, N., Reale, C., Duffy, K. and Gavin, K., 2025. Incorporating spatial variability into finite element analysis of anchored retaining walls. ISGSR 2025: Proceedings of the 9th International Symposium on Geotechnical Safety and Risk. Oslo, Norway.
Hemel, M.J., 2023. Amsterdam quays under pressure: Modelling and testing of historic canal walls. Delft University of Technology, Delft, The Netherlands. PhD Thesis.
Hemel, M.J., Peters, D.J., Schweckendiek, T., Jonkman, S.N., 2024. Reliability updating for lateral failure of historic quay walls. Georisk Assess. Manag. Risk Eng. Syst. Geohazards 18 (4), 882–903. https://doi.org/10.1080/17499518.2024.2302141.
Hicks, M.A., Samy, K., 2002. Reliability-based characteristic values: a stochastic approach to Eurocode 7. Ground Eng. 35.
Hicks, M.A., Spencer, W.A., 2010. Influence of heterogeneity on the reliability and failure of a long 3D slope. Comput. Geotech. 37 (7–8), 948–955. https://doi.org/10.1016/j.compgeo.2010.08.001.
Hu, B., Luo, Z., 2018. Life-cycle reliability-based assessment of internal stability for mechanically stabilized earth walls in a heavy haul railway. Comput. Geotech. 101, 141–148. https://doi.org/10.1016/j.compgeo.2018.04.023.
Kulhawy, F H, Mayne, P W., 1990. Manual on estimating soil properties for foundation design. Electric Power Research Inst., Palo Alto, CA (USA); Cornell Univ., Ithaca, NY (USA). Geotechnical Engineering Group, 1990.
Lai, F., Duffy, K.J., Gavin, K.G., Lu, D., Roubos, A.A., 2025. Integration of field monitoring and numerical modelling to evaluate the construction performance of a deep-sea quay wall. J. Geotech. Geoenvironmental Eng. https://doi.org/10.1061/JGGEFK/GTENG-13694.
Liu, Z., Lacasse, S., Nadim, F., Vanneste, M., Yetginer, G.L., 2015. Accounting for the spatial variability of soil properties in the reliability-based design of offshore piles, in: Frontiers in Offshore Geotechnics III : Proceedings of the 3rd International Symposium on Frontiers in Offshore Geotechnics (ISFOG 2015). Taylor & Francis, Oslo, Norway, pp. 1375–1380.
Matic, I., de Nijs, R., De Vos, M., Roubos, A.A., 2019. Full-scale load testing on long prefabricated concrete piles in the Port of Rotterdam, in: the XVII. In: European Conference on Soil Mechanics and Geotechnical Engineering. Presented at the Proceedings of the XVII ECSMGE-2019, Icelandic Geotechnical Society (IGS), pp. 1–8.
Mayne, P.W., 2005. Integrated ground behavior: In-situ and labs tests. Deformation characteristics of geomaterials. CRC Press, pp. 162-185.
Momeni, E., Poormoosavian, M., Salmani Tehrani, H., Fakher, A., 2021. Reliability analysis and risk assessment of deep excavations using random-set finite element method and event tree technique. Transp. Geotech. 29, 100560. https://doi.org/10.1016/j.trgeo.2021.100560.
Nen, 2017. NEN 9997-1+C2:2017, Geotechnisch ontwerp van constructies - Deel 1: Algemene regels. Nederlands Normalisatie-Instituut, Delft, The Netherlands.
Osório, P., Odenbreit, C., Vrouwenvelder, T., 2010. Structural reliability analysis of quay walls with steel sheet piles. Presented at the PIANC MMC Congress, Liverpool, United Kingdom.
Otake, Y., Honjo, Y., 2022. Challenges in geotechnical design revealed by reliability assessment: Review and future perspectives. Soils Found. 62, 101129. https://doi.org/10.1016/j.sandf.2022.101129.
Pan, X., Jia, J., 2025. Time-dependent system reliability analysis of anchor-reinforced slopes based on surrogate models. Comput. Geotech. 184, 107257. https://doi.org/10.1016/j.compgeo.2025.107257.
Phoon, K.K., 2023. What geotechnical engineers want to know about reliability. ASCE-ASME J. Risk Uncertain. Eng. Syst. Part. Civ. Eng. 9, 03123001. https://doi.org/10.1061/AJRUA6.RUENG-1002.
Phoon, K.K., Cao, Z.J., Ji, J., Leung, Y.F., Najjar, S., Shuku, T., Tang, C., Yin, Z.-Y., Ikumasa, Y., Ching, J., 2022. Geotechnical uncertainty, modeling, and decision making. Soils Found. 62, 101189. https://doi.org/10.1016/j.sandf.2022.101189.
Post, M., Schweckendiek, T., Roubos, A.A., de Greef, J., 2021. Reliability analysis of quay walls: exploring a meatmodelling apporaching for more robustness and efficiency (No. 11204256- 052- GEO- 0003). Deltares, Delft, The Netherlands.
Putteman, J., Broos, E.J., Brassinga, H.E., Spruit, R., De Vos, M., Timmermans, A.L.J., 2019. MV tension pile load tests in the Port of Rotterdam: practical aspects and geotechnical behaviour. ECMGE, in: Proceedings of the XVII ECSMGE-2019. Presented at the XVII European Conference on Soil Mechanics and Geotechnical Engineering, Reykjavik, Iceland.
Rackwitz, R., Flessler, B., 1978. Structural reliability under combined random load sequences. Comput. Struct. 9 (5), 489–494. https://doi.org/10.1016/0045-7949(78)90046-9.
Reale, C., Xue, J., Pan, Z., Gavin, K., 2015. Deterministic and probabilistic multi-modal analysis of slope stability. Comput. Geotech. 66, 172–179. https://doi.org/10.1016/j.compgeo.2015.01.017.
Rippi, A., Nuttall, J., Teixeira, A., Schweckendiek, T., 2016. Uncertainty assessment of a dike with an anchored sheet pile wall using FEM, in: FLOODrisk 2016 - 3rd European Conference on Flood Risk Management. EDP Sciences, Les Ulis, France. doi: 10.1051/e3sconf/20160703020.
Rippi, A., Teixeira, A., 2016. Reliability-based assessment of a retaining wall using FEM, in: Proceedings of the 25th European Young Geotechnical Engineers Conference (EYGEC16). Presented at the 25th European Young Geotechnical Engineers Conference, Sibiu, Romania.
Robertson, P.K., 2009. Interpretation of cone penetration tests - a unified approach. Can. Geotech. J. 46 (11), 1337–1355. https://doi.org/10.1139/T09-065.
Robertson, P.K, Cabal, K.L., 2010. Estimating soil unit weight from CPT. 2nd International symposium on cone penetration testing. 2010: 2-40.
Roubos, A.A., Allaix, D.L., Schweckendiek, T., Steenbergen, R.D.J.M., Jonkman, S.N., 2020. Time-dependent reliability analysis of service-proven quay walls subject to corrosion-induced degradation. Reliab. Eng. Syst. Saf. 203, 107085. https://doi.org/10.1016/j.ress.2020.107085.
Roubos, A.A., Schweckendiek, T., Brinkgreve, R.B.J., Steenbergen, R.D.J.M., Jonkman, S.N., 2021. Finite element-based reliability assessment of quay walls. Georisk Assess. Manag. Risk Eng. Syst. Geohazards 15, 165–181. https://doi.org/10.1080/17499518.2020.1756344.
Roubos, A.A., Steenbergen, R.D.J.M., Schweckendiek, T., Jonkman, S.N., 2018. Risk-based target reliability indices for quay walls. Struct. Saf. 75, 89–109. https://doi.org/10.1016/j.strusafe.2018.06.005.
Ruggeri, P., Fruzzetti, V.M.E., Scarpelli, G., 2019. Renovation of quay walls to meet more demanding requirements: Italian experiences. Coast. Eng. 147, 25–33. https://doi.org/10.1016/j.coastaleng.2019.01.003.
Schmudderich, C., Shahrabi, M.M., Taiebat, M., Lavasan, A.A., 2020. Strategies for numerical simulation of cast-in-place piles under axial loading. Comput. Geotech. 125, 103656. https://doi.org/10.1016/j.compgeo.2020.103656.
Segato, D., Fruzzetti, V.M.E., Ruggeri, P., Scarpelli, E., Sakellariadi, G., 2010. Numerical modelling of a steel sheet-pile quay wall for the harbour of Ravenna, Italy, in: Numerical Methods in Geotechnical Engineering. Presented at the 7th European Conference on Numerical Methods in Geotechnical Engineering (NUMGE 2010), CRC Press, Trondheim, Norway.
Sihombing, R., Tawekal, R. L., Muin, M., Zukhruf, F., 2025. Stochastic optimization model for port infrastructure planning considering uncertainties in wave and vessel arrival times. Int. J. Transp. Sci. Technol. doi: 10.1016/j.ijtst.2025.03.004.
Sluis, J.J.M., Besseling, F., Stuurwold, P.H.H., 2014. Modelling of a pile row in a 2D plane strain FE-analysis, in: Proc. Numerical Methods in Geotechnical Engineering 2014. Presented at the NUMGE 2014, Taylor & Francis, Delft, The Netherlands, pp. 277–282.
Spruit, R., Gavin, K.G., van Dalen, J., Polak, R., Putteman, J., Roubos, A., Westerbeke, F., 2022. Ultimate bearing capacity of MV piles derived from load tests, a suggested new design approach. Presented at the 11th International Stress Wave Conference 2022, Rotterdam, The Netherlands.
Tabarroki, M., Ching, J., Phoon, K.K., Chen, Y.Z., 2022. Mobilisation-based characteristic value of shear strength for ultimate limit states. Georisk Assess. Manag. Risk Eng. Syst. Geohazards 16, 413–434. https://doi.org/10.1080/17499518.2020.1859121.

Tan, H., Jiao, Z., Chen, J., 2018. Field testing and numerical analysis on performance of anchored sheet pile quay wall with separate pile-supported platform. Mar. Struct. 58, 382–398. https://doi.org/10.1016/j.marstruc.2017.12.006.

van den Eijnden, B., Knuuti, M., Lesny, K., Löfman, M., Mavritsakis, A., Roubos, A.A., Schweckendiek, T., Sciarretta, F., Ebener, A., Escher, K., Spross, J., Commend, S., Hehenkamp, M., Arnold, P., Wilhelm, S., Ene, A., Rimoldi, P., Peireira, R., 2024. Reliability-based verification of limit states for geotechnical structures: guidelines for the application of the 2nd generation of Eurocode 7: geotechnical design. Publications Office of the European Union, Luxembourg.

Voogt, H. 2023. Port facilities asset management: Coping with aging infrastructure and constrained budgets on the long term. Life-Cycle of Structures and Infrastructure Systems, 3642-3648, London, UK: CRC Press.

Whitman, R.V., 1984. Evaluating calculated risk in geotechnical engineering. J. Geotech. Geoenviron. Eng. 110 (2), 143–188. https://doi.org/10.1061/(ASCE)0733-9410(1984)110:2(143).

Wolters, H.J., Bakker, K.J., de Gijt, J.G., 2013. Reliability of quay walls using finite element analysis: calibration of partial safety factors in quay wall design by probabilistic Plaxis calculations, in: Proceedings of the 4th International Conference of the Euro-Asia Civil Engineering Forum (EACEF 2013). Institute for Research and Community Service, Surabaya, pp. 37–42.

Yuksel, Y., Tan, R.I., Celikoglu, Y., 2019. Determining propeller scour near a quay wall. Ocean Eng. 188, 106331. https://doi.org/10.1016/j.oceaneng.2019.106331.